A Fuel-Cell-Battery Hybrid for Portable Embedded Systems

Kyungsoo Lee, Naehyuck Chang
Dept. of EECS, Seoul National University
and
Jianli Zhuo, Chaitali Chakrabarti
Dept. of EE, Arizona State University
and
Sudheendra Kadri, Sarma Vrudhula
Dept. of CSE, Arizona State University

This paper presents our work on the development of a fuel cell (FC) and battery hybrid (FC-Bh) system for use in portable microelectronic systems. We describe the design and control of the hybrid system followed by a dynamic power management (DPM) based energy management policy that extends its operational lifetime. The FC is of the proton exchange membrane (PEM) type, operates at room temperature, and has an energy density which is 4 – 6 times that of a Li-ion battery. The FC cannot respond to sudden changes in the load, and so a system powered solely by the FC is not economical. An FC-Bh power source, on the other hand, can provide the high energy density of the FC and the high power density of a battery.

In this paper we first describe the prototype FC-Bh system that we have built. Such a prototype helps characterize the performance of hybrid power source, and also helps explore new energy management strategies for embedded systems powered by hybrid sources. Next we describe a Matlab/Simulink-based FC-Bh system simulator which serves as an alternate experimental platform and that enables quick evaluation of system-level control policies. Finally we present an optimization framework that explicitly considers the characteristics of the FC-Bh system and is aimed at minimizing the fuel consumption. This optimization framework is applied on top of a prediction based DPM policy and is used to derive a new fuel-efficient DPM scheme. The proposed scheme demonstrated up to 32% system lifetime extension compared to a competing scheme when run on a real trace-based MPEG encoding example.

Categories and Subject Descriptors: C [**3**]: Real-time and embedded systems

General Terms: Design, Performance, Measurement, Simulation

Additional Key Words and Phrases: battery, fuel cell, hybrid systems, DPM, and simulator

1. INTRODUCTION

Portable computing and communication devices such as cellular phones, PDAs, palm and laptop computers are fast becoming universally adopted as essential tools of day-to-day

work. The operational lifetime of these devices is determined by the capacity of the energy source, namely, the battery. The capacity of a battery depends on its size, and portability places very stringent constraints on its size, weight, and form factor. Improvements in the energy density of batteries have lagged far behind the increasing energy demand of many portable microelectronic systems. This widening gap between the capabilities of batteries (*energy producer*) and the demands of the processor and peripherals (*energy consumers*) is one of the main challenges in the design of portable systems. Obviously, this gap can be reduced by either improving the energy efficiency of the consumer (performance per Watt) or by increasing the energy density of the producer.

As a result of more than a decade of research, a large body of literature now exists on improving the efficiency of the energy consumers, i.e., processors and peripherals. For processors, the basic techniques involve dynamic voltage and frequency scaling (DVFS) [Burd et al. 2000; Chandrasena and Liebelt 2000; Lu et al. 2002; Simunic et al. 2001; Yan et al. 2003; Choi et al. 2004; Ishihara and Yasuura 1998; Cho et al. 2006] and for subsystems such as disk drives and other peripherals, the methods involve various forms of *speed* control, and are generally referred to as dynamic power management [Benini and De Micheli 1998; Pedram and Rabaey 2002; Rabaey and Pedram 1995; Lu et al. 2000b; Kelly 2004; Macii 2004]. Power consumption still continues to plague the industry due to the continuing increase in leakage current. The alternative is to improve the energy density of the producer. An excellent alternative to a battery, and one which can provide the energy densities required by portable computing and communication devices of the future, is a fuel cell (FC).

A FC is an electrochemical device that uses hydrogen (H_2) and oxygen (O_2) to generate electrical power. FCs are environmentally clean (by-product is water and heat), safe, provide instant power (no recharging), can be highly modular (configurable for a wide range of outputs), and provide very high energy densities as compared to batteries [Nasiri et al. 2004a]. For instance, a Li-ion battery pack used in cellular phones has a typical volumetric energy density of 250 Watt-hours per liter (Wh/l), with a theoretical upper limit of 480 Wh/l [Xie et al. 2002]. A methanol based FC and a H_2 based FC (using sodium borohydride) have a volumetric energy density of 4780 Wh/l and 7314 Wh/l, respectively [Xie et al. 2002]. Even assuming 20% efficiency when converting chemical to electrical energy, these FCs have energy densities ranging from 1000 – 1500 Wh/l - more than 4X of the energy density of today's Li-ion battery. Small-size room temperature FCs such as a PEMFC (proton exchange membrane FCs) powered by H_2 and a DMFC (direct methanol FC) powered by methanol, are under development for portable applications where the power range is the order of 1 – 100 W [Xie et al. 2002; Palo et al. 2002].

Our FC-Bh system consists of a sodium borohydride ($NaBH_4$) PEMFC system that works at room temperature, and two Li-ion batteries. We have developed a unique architecture for the hybrid operation and proposed new charge management schemes. We have built a hardware platform to demonstrate the use of an FC-Bh system for human-portable embedded applications, and to characterize the FC-Bh system. We have also built a simulator that enables quick evaluation of the policies for FC-Bh system control and management.

A study of the characteristics of the FC-Bh system brought to light several significant differences with battery powered systems. First, the efficiency of the FC is a function of the load current and is independent to the amount of remaining fuel, in contrast to batteries

whose performance is primarily affected by the remaining energy. Second, the limited power capacity of the FC restricts the range in which the FC can track the load. Even in this restricted range, the *load following* is not automatic, and has to be controlled by explicit fuel flow rate control. As a result, energy management policies that enhance the lifetime of battery-powered systems are not directly applicable to an FC-Bh power source. In this paper, we present a dynamic power management (DPM) based energy management policy that maximize the operational lifetime of the embedded system powered by the FC-Bh system. We developed an optimization framework that explicitly takes into account the characteristics of the FC-Bh system. This framework is utilized in the development of a new prediction-based DPM algorithm. The algorithm was evaluated using a real trace-based MPEG encoding example and demonstrated up to 32% enhancement in the system lifetime.

The rest of the paper is organized as follows. An overview of an FC-Bh system is given in Section 2. This includes basic FC stack operation (2.1), FC-Bh system overview (2.2), FCs for human-portable applications (2.3), and on-site H_2 generation (2.4). Section 3 describes the FC control and charge management including FC-Bh prototype description (3.1), FC-Bh operation schemes (3.2), and battery charging methods (3.3). Section 4 gives a detailed analysis of FC-Bh operation including the step response analysis (4.1) and efficiency analysis (4.2). Section 5 presents the FC-Bh system simulator based on Matlab/Simulink. Section 6 introduces a new FC-aware DPM algorithm followed by its evaluation. Section 7 concludes the paper.

2. PORTABLE FC-BH SYSTEMS

2.1 FC operation basics

FCs are typically classified based on the type of electrolyte [Larminie and Dicks 2000]. For portable applications, the key candidates are PEMFC and DMFC since they can be operated at low temperature ($< 70\ ^\circ$C). A PEMFC transforms the chemical energy liberated during the electrochemical reaction of H_2 and O_2 to electrical energy without combustion. A DMFC can be classified as a PEMFC, but in general a distinction is made between the two. In a DMFC, methanol is not reformed but fed directly to the membrane, while a PEMFC uses H_2 as the fuel.

We focus on PEMFC since it has high performance and is also cost effective. In fact, a PEMFC requires only 0.2 mg/cm^2 of platinum catalyst [Akbari 2005] compared to a DMFC which requires significantly large amounts, usually 4 to 8 mg/cm^2 [McGrath 2006]. Recently, SOFCs are being seriously considered since they do not require complicated water management and precious metal catalyst such as platinum, and can be operated with commercial fuels. Since these fuel cells operate at temperatures ranging from 650 to 800 $^\circ$C, novel heat sealing techniques are being proposed for their use in portable applications. Note that the approach in this paper is not limited to only PEMFCs, and can be applied to other FCs for portable applications.

In its simplest form, a PEMFC has two electrodes (anode and cathode) separated by an ion conducting membrane. The fuel is fed to the anode and O_2 is fed to the cathode. At the anode, the reaction is given by

$$H_2 \rightarrow 2H^+ + 2e^-, \tag{1}$$

i.e., a H_2 molecule splits into H^+ ions and e^- electrons. The H^+ ions move towards

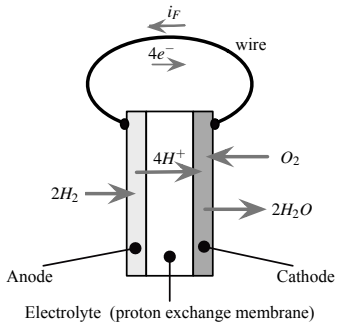

Fig. 1. The basic reaction in a FC.

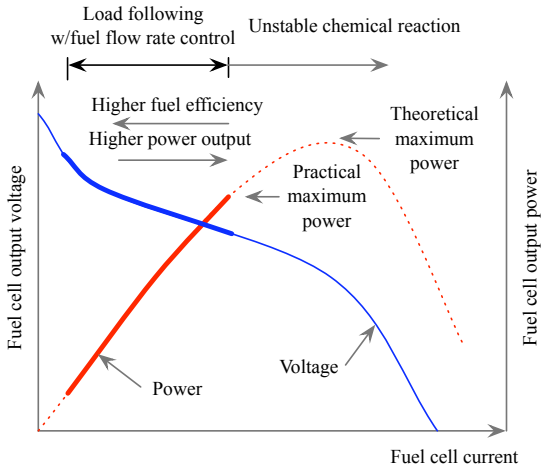

Fig. 2. Polarization curves for a PEMFC.

the cathode through the ion conducting electrolyte (membrane). The e^- electrons find a different path to the cathode, namely, through the external wire that connects the anode and the cathode. At the cathode, the reaction is given by

$$2H^+ + 2e^- + \frac{1}{2}O_2 \rightarrow H_2O, \tag{2}$$

producing water as a by-product. The reaction inside the FC needs water and heat, and so the membrane of the FC stack must be moist. A complete FC system thus requires a thermal and hydration management system to maintain the required temperature and hydrating condition, and also the capability to remove excessive heat and water. Also, many FC systems use air to provide O_2 to the cathode, and so require an air management system to ensure that the O_2 supply is in abundance.

Fig. 2 shows a typical plot of the voltage and power versus current of a PEMFC. As the current density increases, the open circuit voltage (about 1.2 V per cell) reduces. The

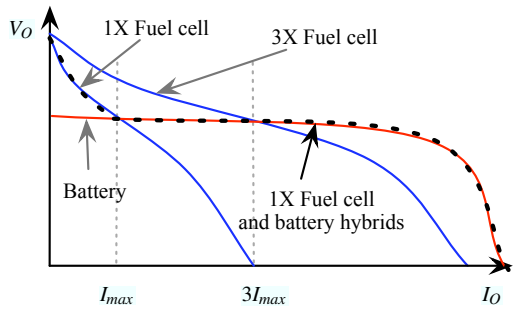

Fig. 3. Advantage of using an FC-Bh power source over a FC-only source.

maximum FC output current is determined by the current density of the membrane times the area of the membrane. The FC output voltage is determined by the single cell voltage times the number of stacked cells. The FC output power can be varied with a given range, referred to as the *load following* region, by controlling the fuel flow rate. In fact, the FC output power depends on temperature, pressure and humidity, and these need to be dynamically controlled for maximum efficiency [Nasiri et al. 2004b; Gielniak and Shen 2004; Ozatay et al. 2004].

2.2 FC-Bh power sources

In this section, we describe an FC-Bh power source where the FC is the primary power source and provides the average power, and the battery is the secondary source and supplies the additional power (peak power) to support the fluctuation. Such a system is very efficient since it provides the high energy density of FCs and the high power density of batteries [Jiang et al. 2005; Jarvis et al. 2002]. Furthermore, such a system not only improves the power capacity and response time, but also can be built with smaller components. Note that the secondary power source could be a battery or a super capacitor [Gao 2005] or a combination [Zheng et al. 2001] of both.

Fig. 3 shows a situation where the maximum load current is 3X. If the power source was only a FC, then it would be designed to accommodate the worst case load (the 3X FC), requiring a larger and heavier unit. On the other hand, the FC unit in a hybrid system can be designed for the average case, with a small battery providing the additional current when needed. The superiority of an FC-Bh power source over FC-only power sources has been demonstrated in terms of system efficiency, dynamic control requirement, etc., in [Guezennec et al. 2003; Vahidi et al. 2004; Vahidi et al. 2005]. It is the structure of choice for powering future high performance portable microelectronic systems [Jiang et al. 2005; Jarvis et al. 2002; Gao et al. 2005; Guezennec et al. 2003; Nasiri et al. 2004b; Zheng et al. 2001].

2.3 FCs for human-portable applications

FC technology has advanced rapidly in the past decade. Most of the advances have come from industries' focus on distributed power generation and automotive applications, where the power range is of the order of 1 – 10 MW and 1 – 10 KW, respectively. Recently, significant efforts are underway to design FCs for the portable consumer electronics market

where the power range is the order of 1 – 100 W. For human-portable applications, FCs have to be operational at relatively low temperatures.

FCs for portable applications are being built by many companies, including Casio (Japan), Motorola (US), Nokia (Europe), Samsung (Korea), etc. Several operational prototypes based on DMFCs have been reported, including a sub-one W power unit by Motorola [Xie et al. 2002], a miniaturized PEM methanol-based FC with 0.5 to 20 W of power for powering portable telecommunication and computing devices [Maynard and Meyers 2002], and a 15 W unit that consists of a H_2-generating fuel reformer coupled to a PEMFC [Palo et al. 2002].

Much of the prior work on the control of FC-Bh systems has been in the context of automobiles. There are two possible arrangements of the FC and battery within a hybrid system: a *passive* mode in which the FC and the battery are connected directly to the power bus, and an *active* mode, in which a DC-DC converter and a sophisticated controller is inserted between the FC and the battery [Gao et al. 2005; Jiang et al. 2005]. While the passive mode is simple and can be used in portable systems, the battery connected to the power bus is either in the discharge mode or in the trickle charge mode, and results in inefficient use of charge generated by the FC.

The active methods developed for automotive applications are not directly applicable to FC-Bh powered portable systems. For automobiles, the primary load is a traction motor, which can be either a power consumer during acceleration or a power generator during braking. Typically, the current generated during braking is dissipated with a braking resistor, though more recently, charge management systems have been developed where the batteries are charged with the generated current. In contrast, in portable embedded systems, the system is always a power consumer, which seems an easier design problem at first glance. But, there are substantial differences between the two systems which make the charge management for FC-Bh system used in embedded systems quite challenging.

In automotive systems, the load demand is generally a soft constraint. Failure to accurately follow the load results in lack of traction power which might be an inconvenience to the driver but does not result in a technical system failure. In contrast, the load demand of an embedded system is a hard constraint, and its violation is likely to result in a critical system failure. Secondly, the load dynamics in embedded systems is orders of magnitude faster; this makes the fuel flow control and the charge management quite complicated. Most importantly, the automotive systems are simply reactive and the required load current acts as a reference signal that the hybrid power system must track faithfully. In contrast, in embedded systems, as long as the task deadline is met, appropriate speed control can be applied to reduce its power consumption. So the best charge management policy for portable embedded systems does not only track the load profile, but also actively reshapes the load profile. We have presented procedures for reshaping the load profile based on a combination of FC control and embedded system power management using DVS [Zhuo et al. 2006a; 2006b] and DPM [Zhuo et al. 2007a; Zhuo et al. 2007b].

2.4 H_2 generation for portable applications

H_2 storage is one of the key issues in the design of PEMFCs. This is even more crucial for human-portable FCs where a H_2 canister cannot be easily employed due to safety and weight considerations. Although, recently there have been novel attempts to develop micro H_2 canisters [JSW 2007], onsite H_2 generation is still the preferred mode of operation. H_2 can be stored in many different forms – as compressed or liquefied H_2 in tanks, by

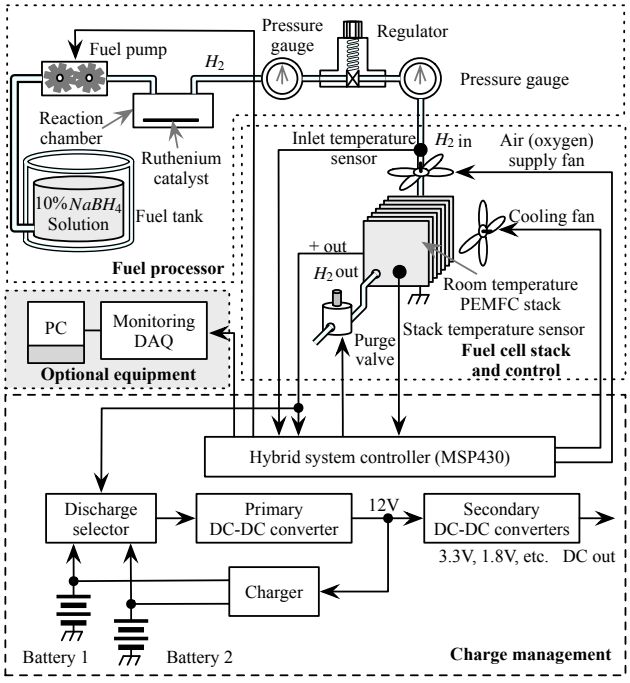

Fig. 4. Architecture of the FC-Bh system.

adsorption on activated carbon and carbon nanotubes, in a H_2-absorbing alloy, as chemical hydrides including $NaBH_4$, NaH, LiH, $NaAlH_4$, MgH_2, $LiBH_4$ and metal nitrides, or as organic hydrides (methylcyclohexane or decahydronaphthalene). Recently, much attention has been given to H_2 generation by the hydrolysis of a chemical hydride, in particular, sodium borohydride ($NaBH_4$), because of its stability and easy conversion to H_2 by a catalyst [Kojima 2005; Gervasio et al. 2005]. In this paper, we also consider $NaBH_4$ as the H_2 fuel. The chemical reaction for H_2 generation is as follows:

$$NaBH_4 + 2H_2O \xrightarrow{Ru} 4H_2 + NaBO_2 + 218kJ/mol. \quad (3)$$

The catalyst for the chemical reaction is ruthenium (Ru). This chemical reaction generates warm and humid H_2 which is particularly conducive to the chemical reaction in the FC (given by Equations (1) and (2)). This is one more reason why sodium borohydride is one of the most promising fuels for PEMFCs.

3. FC-BH SYSTEM DESIGN AND IMPLEMENTATION

3.1 FC-Bh system prototype

We have built a prototype system that uses a room temperature, self-humidifiable, 20 cell 20 W stack manufactured by BCS FC Systems [BCS 2006]. The open-circuit output voltage of the BCS PEMFC stack is 18 V. The structure of the hybrid system is shown in Fig. 4. It consists of three subsystems: the fuel processor, the FC stack and control, and the CMS. The fuel processor is responsible for supplying the H_2. The FC stack and control subsys-

tem consists of the PEMFC stack, a microprocessor, sensors (temperature and pressure) and actuators (fans and a purge valve solenoid). The CMS delivers the required power to the embedded system. Its functions include discharge scheduling (discharging the FC, battery or both simultaneously), and battery charge scheduling.

The BCS PEMFC stack requires 2 to 3 psig H_2 pressure in the anode. When $NaBH_4$ solution is supplied to the reaction chamber of the fuel processor, the chemical reaction is activated by Ru and H_2 is generated. The amount of $NaBH_4$ delivered, determines the amount of H_2 generation. Because of significant fluctuations in pressure, we use a pressure regulator to regulate the H_2 pressure in the anode, with 2 psig as the default value. Typically, a miniature gear-driven or cam-driven electric motor pump or piezoelectric pump is used for the fuel pump. We use a micro piezoelectric pump (25 mm $\times$ 25 mm $\times$ 4.8 mm) with the flow rate of 7 ml/min and the power consumption of 240 mW [STA 2007]. As 2 to 3 psig H_2 pressure is formed at the anode, a similar amount of O_2 pressure is required at the cathode. While a piston- or a diaphragm-type air compressor is used for high-pressure FC stack operation ($>$ 4 psig) that has an O_2 channel, here we use a blower fan to deliver O_2 since the cathode of the BCS PEMFC stack is exposed to the outside.

The efficiency of the FC stack is dependent on the temperature and so the stack temperature must be maintained at a particular value (45°C for the BCS PEMFC stack) for maximum efficiency. Generally the FC stack has less than 50% efficiency, since more than half of the chemical energy becomes heat. It is possible to cool down a FC below 100 W purely with convective air [Larminie and Dicks 2000], but we use a cooling fan for robust operation against the ambient temperature variation. The maximum allowable temperature of the BCS 20 W FC stack is 65 °C.

We operate the FC stack with a dead-end anode configuration; i.e., the H_2 flows into the anode with nowhere to go except through the membrane. This creates a sufficient back pressure that provides an automatic regulation of the inflow of H_2. While this is more efficient than an open-end configuration, it may generate excessive water that blocks the H_2 channel. Hence it is necessary to periodically flush (or purge) water by opening the purge valve, often implemented with a normal-closed type solenoid valve at the end of the H_2 channel. On the cathode side, we use two fans to control the air (O_2) flow into the cathode as well as maintain the stack temperature.

The main controller unit is equipped with an ultra-low-power microcontroller, TI MSP430FG438 that operates at 8 MHz and consumes a mere 300 μW/MIPS. The main controller unit also has a constant-current and constant-voltage Li-ion battery charger with a maximum charging current of 2 A, and three PWM drivers with a frequency of operation of 20 KHz. The final output DC-DC converter can be selected depending on the voltage requirement of the target embedded system (Fig. 4).

Our hybrid system control software has been designed to operate on a tiny real-time OS, called μC-OS II. The μC-OS II is small enough to be squeezed into 2KB of code space, and thus is suitable for MSP430FG438 with small on-chip memory. The control program consists of five main threads for the system boot up, temperature control, water management, monitoring, and housekeeping. The system control software is connected to a PC Windows program for system monitoring. Fig. 5 shows a photograph of the prototype that we built and demonstrated.

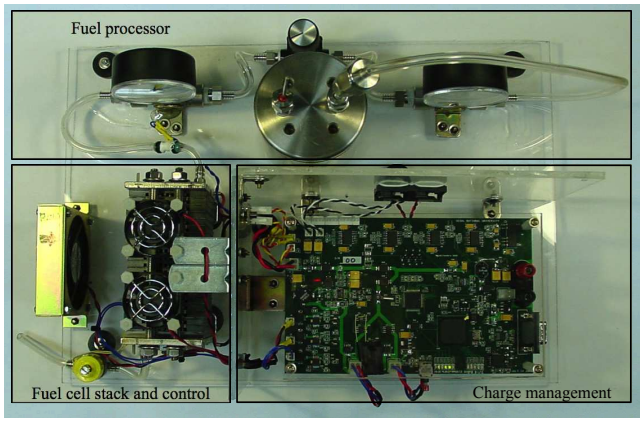

Fig. 5. Photograph of the FC-Bh system demonstrated at SIGDA University Booth 2006, Station 4, Demo 22.

3.2 Proposed FC-Bh operation

In an FC-Bh system, the embedded system can be powered by the FC or battery or both. An appropriate hybrid operation makes it possible to use a very small size battery in comparison with battery-only systems, and also to use a smaller size FC in comparison with FC-only systems. The simplest way is to use the FC only for charging the battery, and to use the battery to supply power to the embedded system. This is a simple replacement of a conventional AC charger with a FC, and does not require modification of existing hardware. However, in this case, the battery is in discharge mode at all times and affects the battery cycle life. Also, the maximum power capacity of the hybrid system is limited by the battery power capacity. Also the desirable battery size is similar to that of battery-only systems.

Next we describe four schemes for more practical hybrid operations. The *static selection* scheme shown in Fig. 6(a) powers the embedded system with either the FC or the battery. When the load current is lower than the maximum FC current, the embedded system is powered by the FC, and when the load current exceeds the maximum FC current, the selection switch changes the power source from the FC to battery. The battery is charged by the FC when the load current is smaller than the maximum FC current [Jiang et al. 2005]. Static selection is also easy to implement with a commercial-off-the-shelf component such as LTC1479. The static selection does not use the batteries continuously as in the former case, but here too the capacity of the hybrid system is limited by that of the battery. Also, the battery size cannot be reduced significantly.

The ideal hybrid operation is to use the FC to supply bulk of the power and to compensate the shortage (when the load current is larger than the maximum FC current) with a battery. In this case, the size of battery can be much more smaller than that of the static selection scheme. This can be partially achieved by a *dual-input flyback transformer* [Kippley 2004] that allows simultaneous discharge from the battery and the FC, as shown in Fig. 6(b). The maximum power capacity of this structure is the sum of the FC capacity and the battery capacity. Unfortunately, this method uses a multiple-input fly-back DC-DC converter which is expensive compared to conventional buck converters and is also not

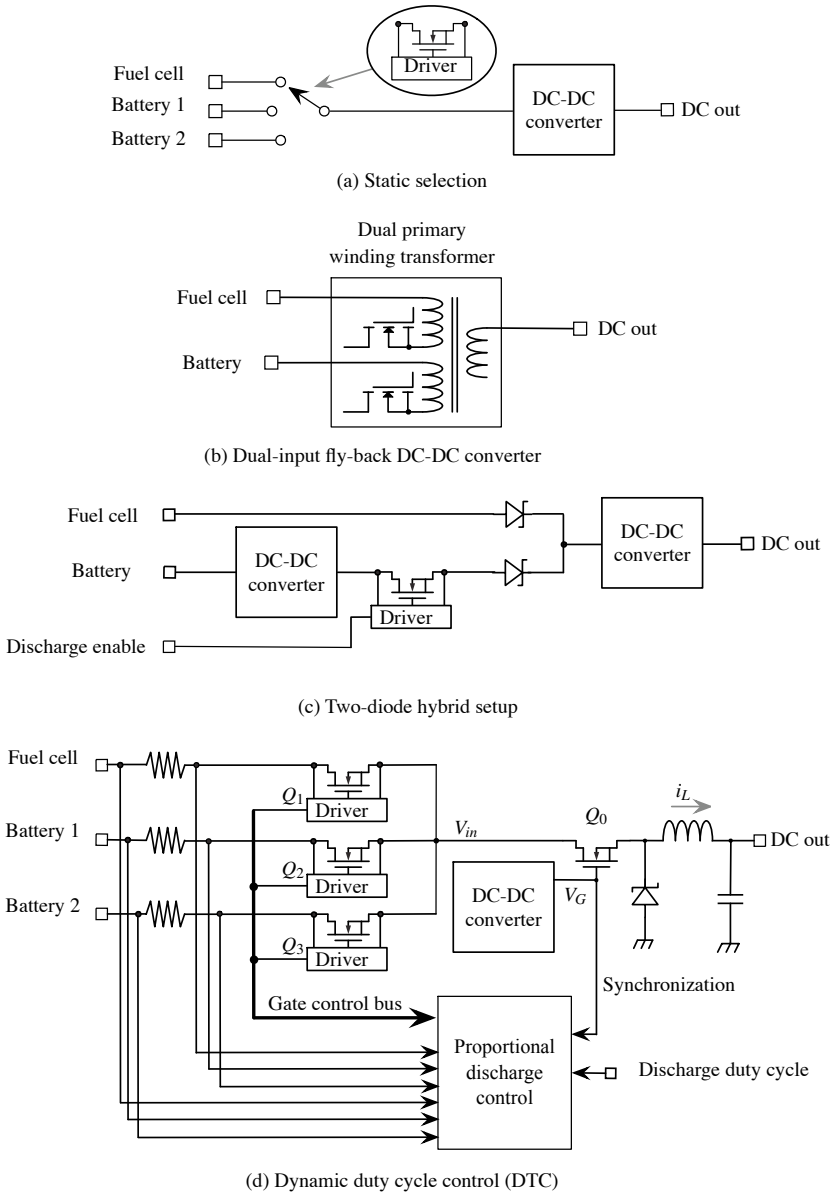

(a) Static selection

(b) Dual-input fly-back DC-DC converter

(c) Two-diode hybrid setup

(d) Dynamic duty cycle control (DTC)

Fig. 6. Utilizing multiple power sources to generate a single power output.

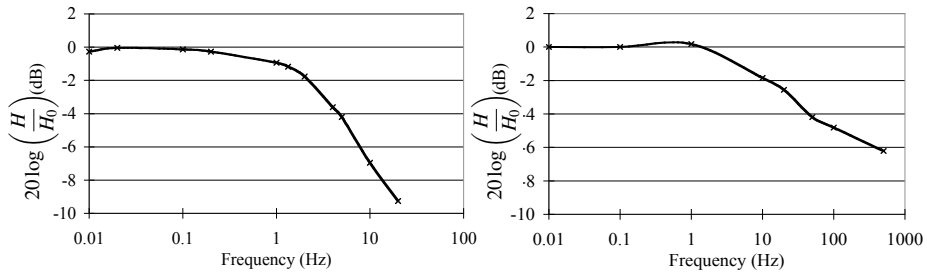

(a) Frequency response of the fuel cell stack (b) Frequency response of the Li-ion battery

Fig. 7. Frequency response of FC and battery.

commercially available.

In this paper we introduce two new active hybrid operation schemes. We first introduce a *two-diode* scheme (Figs. 6(c)) that offers the same functionality as the dual-input flyback DC-DC converter. The two-diode scheme enables us to use a conventional buck DC-DC converter with only two more diodes. If the load current is smaller than the FC maximum current, the FC output voltage drops below the battery voltage. This automatically increases the battery discharge current. However, the two-diode scheme needs additional DC-DC converter between the battery and diode, and the loss in the additional DC-DC converter and diode is not negligible.

Next, we propose an advanced hybrid operation scheme based on a buck converter, and free from the diode power loss. It allows a greater degree of freedom in controlling the proportion of the discharge current from each power source and is very efficient. We refer to this scheme as *Dynamic duTy cycle Control (DTC)*. The schematic diagram of DTC is shown in Fig. 6(d). The selection switches, Q_1, Q_2 and Q_3, operate at a high frequency and are synchronized to the gate control signal of Q_0. We change the on/off states of Q_1, Q_2 and Q_3, when the MOSFET Q_0 is closed. The duty cycle (on state) of Q_1, Q_2 and Q_3 determines the proportion of the current flow of each power source like PWM (pulse width modulation).

The prototype FC-Bh system that we have built uses DTC. Since efficiency of the DTC operation is strongly dependent on the switching frequency of the input selection MOSFETs, we determined the switching frequency based on the frequency response of the FC and battery. Fig. 7 describes the frequency response obtained by intensive measurement. Both the cut-off frequencies of the FC and battery are lower than 10 Hz, and thus using a switching frequency higher than 10 Hz does not change the efficiency of the FC and battery. We use LT1769 for the primary DC-DC converter that requires an off-chip power MOSFET (Q_4 in Fig. 6). We utilize its gate drive signal to synchronize the input MOSFET switches for the DTC (Q_1, Q_2 and Q_3 in Fig. 6). The input switching frequency of Q_1, Q_2 and Q_3 is 200 Hz in our design.

3.3 Battery management

Li-ion batteries and super capacitors are commonly used as charge buffers for alternative power sources [Simjee and Chou 2006]. Super capacitors are not subjected to the cycle-life problem, but they have problems of leakage current. Also, their output voltage is

linearly proportional to the amount of charge stored, which makes the design of the DC-DC converter and charger circuit particularly challenging.

One of the main disadvantages of Li-ion batteries is that they have limited cycle life ($<$ 500 deep cycles). In a single battery system, the Li-ion battery discharges whenever the load current exceeds the maximum FC current and charges when the load current is lower than the maximum FC current. As a result, the battery goes through repeated charging and discharging cycles. A dual battery scheme can mitigate the cycle life degradation. Once a battery is set to the "charge" mode, it continues to be in this mode till it is fully charged. It then switches to the "discharge" mode and continues to be in this mode till the other battery is fully charged. Once a battery is fully charged, it goes into discharge mode even though the other battery has not been fully discharged. This scheme can significantly reduce the number of state changes of the battery and enhance its lifetime.

Li-ion batteries should not be overcharged or over discharged to avoid degradation of the cycle life as well as possible explosion. While a Li-ion battery has internal protection circuits, strict control is required to ensure that the specifications are not violated, i.e., the limits on maximum charging or discharging current, maximum charging voltage, and minimum discharging voltage are not exceeded. The Li-ion battery used in our platform consists of 3 cells providing a total of 850 mAh. This battery is optimized for large discharge current of the order of 8.5 A current, i.e., 10 C. Also it can be charged with up to 850 mA current, i.e., 1 C, and the corresponding end-of-charge voltage is 12 V.

In our system, for higher efficiency, the battery is first charged with constant current until the output voltage reaches 12 V. Then the charging method is changed to constant voltage mode with the terminal voltage maintained at 12 V. At the end, when the battery is fully charged, the battery charging current is 0 A, and the output voltage is 12 V.

The amount of charging current is controlled by a microcontroller using a digital potentiometer connected to a battery charger. The charging current is limited by 750 mA, slightly below the maximum allowed charging current (1 C). The battery output voltage level is recorded periodically by an analog-to-digital converter embedded in the microcontroller. If this parameter reaches 12 V, the microcontroller changes the charging method from constant current mode to constant voltage mode using a GPIO connected to the charger IC.

4. FC-BH SYSTEM ANALYSIS

4.1 FC-Bh system performance: step response

For linear time invariant systems, the step response can be used to characterize the system transfer function. Fig. 8(a) shows the step response with a 15 W load. Since 15 W is almost the upper limit of the power capacity of the FC with 2 psig H_2 supply, the output voltage for this configuration is quite unstable. Such an unstable and nonlinear step response makes the controller design very difficult in general. The voltage fluctuations (comb-like spiky voltage drops) shown in the figure are caused by the purge operation. Fig. 8(b) shows the same 15 W load step response of the hybrid system whose CMS was designed with DTC. The output voltage is almost flat because of the voltage versus load current characteristic of the battery.

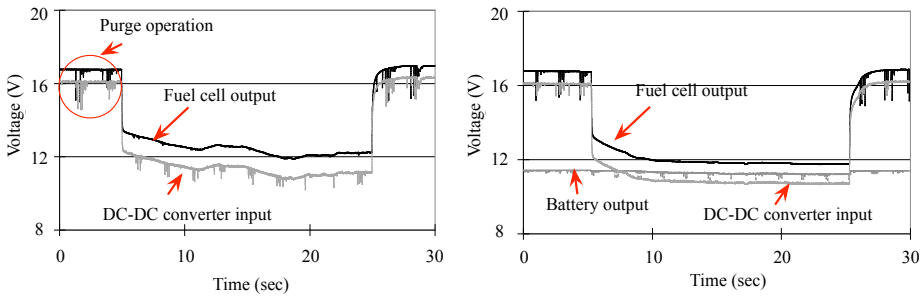

(a) Fuel cell only system (b) Hybrid system

Fig. 8. Step response of FC-only and hybrid systems.

4.2 FC-Bh system efficiency

The FC stack efficiency is best described in terms of Gibbs free energy, unlike heat engines which are explained in terms of Carnot limit. The Gibbs free energy, $\mathcal{G}$ is a thermodynamic potential which measures the maximum amount of work extracted from a closed system. It is represented by

$$\mathcal{G} = \mathcal{U} + PV - T\mathcal{S}, \tag{4}$$

where P is the pressure, V is the volume, T is the temperature (K), $\mathcal{U}$ is the internal energy, and $\mathcal{S}$ is the entropy (J/K) [Perrot 1998]. The FC stack efficiency is defined as the ratio of the electrical energy to the Gibbs free energy [Larminie and Dicks 2000]:

$$\text{FC stack efficiency} = \frac{\text{Electrical energy produced}}{\mathcal{G} \text{ change}}. \tag{5}$$

Here the electrical energy is the integration of the product of the FC stack current and voltage with time. The amount of Gibbs free energy change is the fuel consumption, i.e., the number of H_2 molecules consumed. The number of H_2 molecules is exactly proportional to the number of electrons. Thus the FC stack efficiency has the same trend as the stack output voltage.

The FC system efficiency is a function of not only the FC stack efficiency but also the power consumption of the FC system controller and the DC-DC converter efficiency. Among the controller components mentioned in Section 3.1, the cathode air blower fan and the cooling fan consume significant power, and thus seriously affect the FC system efficiency. Their power consumption is strongly dependent on the size and type (blower, diaphragm, piston, etc.) as well as the type of control method. In this paper, we compare two control methods. A constant-speed fan control, which is simple and suitable for low-cost systems, and a variable-speed fan control that performs speed control of the fan according to the O_2 consumption, or equivalently, the FC current. Like the cathode fan, the power consumption of the cooling fan depends on the size and type of the fan as well as the control method. Note that the cooling fan power is also strongly dependent on the airflow design.

The DC-DC converter efficiency also has a strong effect on the FC system efficiency. Most DC-DC converters have 80% to 90% efficiency for a medium load current, and lower efficiency for a light or a heavy load. Fig. 10 shows measured efficiency of DC-DC con-

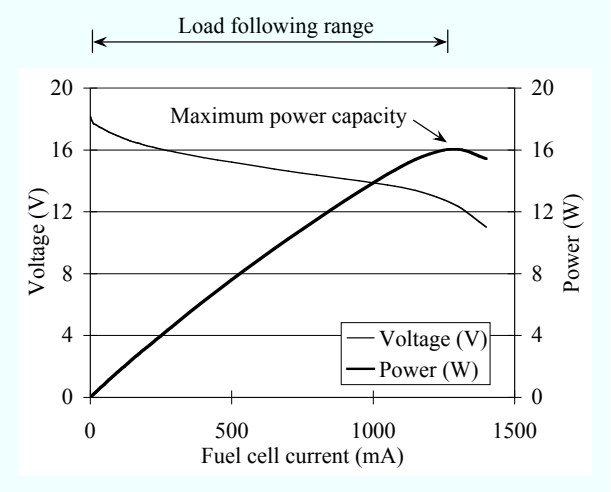

Fig. 9. Measured output voltage and power versus load current characteristics of the BCS 20 W, 20 stack, room-temperature PEMFC (@2 psig H_2 pressure).

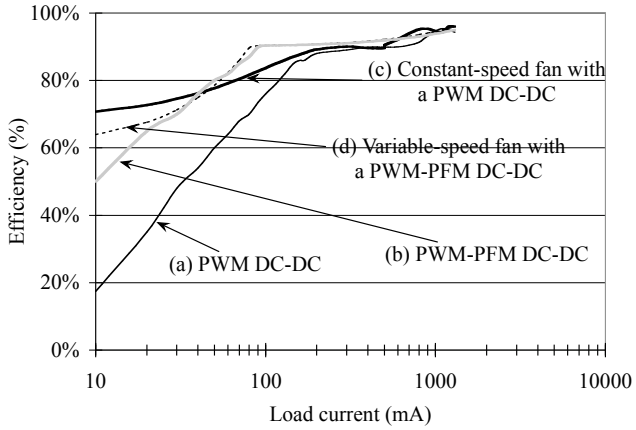

Fig. 10. Measured efficiency of DC-DC converters: LTC1625 (PWM) and LTC3780 (PWM-PFM).

verters that use PWM and PWM-PFM (pulse-frequency modulation). With a light load ($<$ 100 mA), the measured efficiency of a typical PWM DC-DC converter ranges from 20% to 70% (Fig. 10(a)), while a PWM-PFM (pulse-frequency modulation) DC-DC converter has 50% to 80% efficiency (Fig. 10(b)).

When the embedded system draws small current, the DC-DC converter efficiency is dependent on the fan power consumption. Note that a constant-speed fan with a PWM DC-DC converter (Fig. 10(c)) shows better efficiency than a variable-speed fan with a PWM-PFM DC-DC converter (Fig. 10(d)) for a light load ($<$ 50 mA) because the fan power consumption becomes a bias current that enhances the DC-DC converter efficiency. However,

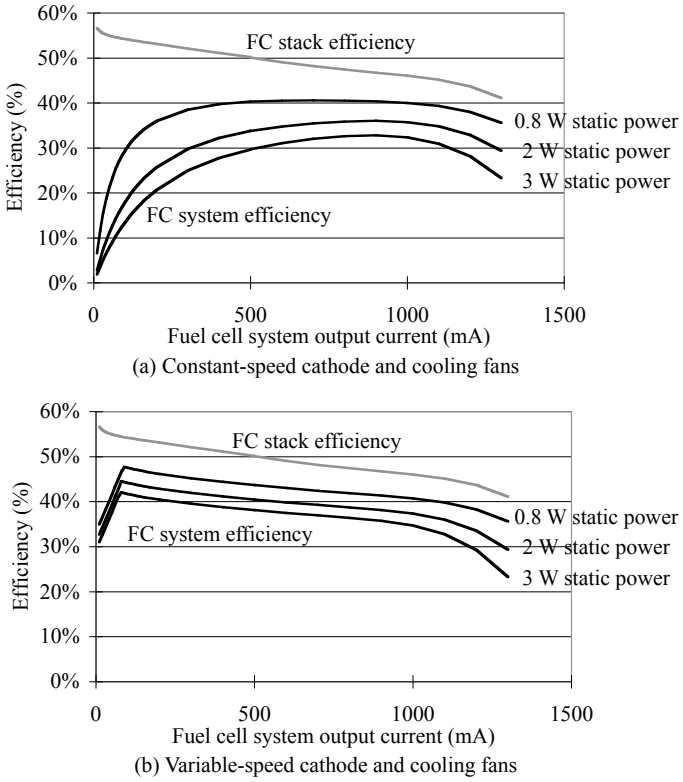

Fig. 11. Measured FC stack efficiency and FC system efficiency. Static power is the summation of the power consumption of all the controller components, where the cathode fan power and cooling fan power are dominant.

this does not imply that a PWM DC-DC converter with constant fan speed (Fig. 10(c)) is more desirable than a PWM-PFM DC-DC converter with variable fan speed (Fig. 10(d)) because the actual power loss is the fan power consumption times the DC-DC efficiency.

The rest of the components consume little power, and their contribution to the FC system efficiency is minor. The fuel pump power is negligible even though we use a motorized pump. A piezoelectric pump consumes even less amount of power. The purge valve is a solenoid, which is supposed to consume 0.67 W to open it, but since it is operated for around 0.35 s every 5 min, its average power is quite small. Finally, the TI MSP430 microprocessor is an ultra-low-power microprocessor which consumes about 10 mW at 8 MHz clock. The charge loss in the charge storage elements is highly dependent on the manufacturer as well as the charging method. In this paper, we assume that there is no charging/discharging loss in the charge storage element.

Fig. 11 shows the whole FC system efficiency as a function of the output current. The overall system efficiency is worse than the FC stack efficiency, as expected. We see that the constant speed fan control is good enough when the minimum load current is larger than 30% of the maximum as shown in Fig. 11(a). However, if the FC system frequently operates below 30% of the maximum current, variable-speed fans are more efficient as

shown in Fig. 11(b).

Embedded systems which implement DPM for energy management benefit by using an FC-Bh system with variable speed-fans. This is because DPM policies tend to aggregate the active periods (or idle periods), resulting in high load current variation. When the load current is small, the FC-Bh system has high efficiency (low power loss). In contrast, energy management policy such as dynamic voltage scaling (DVS) tends to flatten out the load current. For such configurations, a constant-speed fan setup gives reasonable efficiency in spite of its simple structure and has been used in [Zhuo et al. 2006b].

In this paper, we use a PWM-PFM DC-DC converter and variable-speed fans, where the fan speed is proportional to the load current. The measured FC system efficiency for this configuration is shown in Fig. 11(b). The system efficiency is now a function of the load current, I_O. In the load following range under consideration ($I_O \in [0.1, 1.2]$A), the system efficiency η_s drops from 46% to 30%. This can be characterized by a simple linear model

$$\eta_s \approx \alpha - \beta I_O, \tag{6}$$

where α and β are positive coefficients determined by the measured efficiency curve.

The relation between I_F (FC stack current in Fig. 4) and I_O can be derived from Equations (5) and (6), and expressed as

$$I_F = \frac{V_O \times I_O}{\zeta \times \eta_s} = \frac{V_O \times I_O}{\zeta \times (\alpha - \beta I_O)}, \tag{7}$$

where V_O is the primary DC-DC converter output voltage (Fig. 4), which is 12 V. It turns out that $\zeta \approx 37.5$ after measurement, and we have

$$I_F = 0.32 \times \frac{I_O}{\eta_s} = \frac{0.32 \times I_O}{\alpha - \beta I_O}. \tag{8}$$

This efficiency model has been used in deriving the FC-aware DPM policy in Section 6.

5. FC-BH SYSTEM SIMULATOR

Along with the hardware platform, a FC-Bh system simulator has been built using Matlab/Simulink (Fig. 12). The simulator contains analytical models of the FC, battery, fan, solenoid, pump, CMS, and DC-DC converter. It provides a platform to evaluate the performance of a given application under various configurations of the FC-Bh system. For instance, the simulator enables us to change the FC-Bh system configuration such as the FC stack capacity, the number of stacks, the capacity of the battery, the number of batteries, etc., so that it meets the system specifications. Furthermore, it allows us to evaluate various power management algorithms for embedded systems powered by the FC-Bh system. The model parameters have been tuned by measurement data from the FC-Bh system platform.

FC stack: There are detailed low level models based on partial differential equations as well as high level empirical models for the FC stacks. Our simulator incorporates the empirical models described in [Pukrushpan et al. 2004]. We assume without loss of generality, that for a 20 cell stack FC, the H_2 pressure, air pressure, humidity, stack temperature, and membrane water content are constant.

The model calculates the FC voltage v_{fc} for the given current i, and the H_2 flow

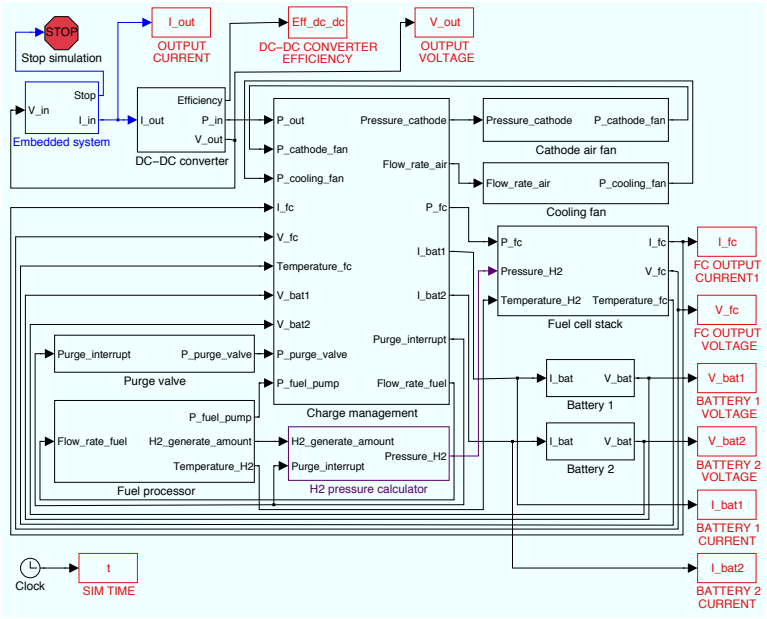

Fig. 12. FC-Bh system simulator in Matlab/Simulink.

rate (Kg/s) (rate of H_2 consumption by the application). The FC voltage is given by

$$v_{fc} = 1.229 - 0.85 \times 10^{-3}(T_{fc} - 298.15) + 4.3085 \times 10^{-5} T_{fc} \left(\ln(P_{H_2}) + \frac{1}{2} \ln(P_{O_2}) \right) - \frac{RT}{2\alpha F} \cdot ln(\frac{i}{i_0}) - iR_\Omega - B \cdot ln\left(1 - \frac{i}{i_{max}}\right), \quad (9)$$

where T_{fc} is the temperature of the FC (in Kelvin), P_{H_2} and P_{O_2} are the partial pressure of the H_2 and O_2, expressed in atm, R is the gas constant, T is the stack temperature, α is the charge transfer coefficient which is different for the anode and the cathode, i_0 is the exchange current density which is again different for both the anode and the cathode, B is a parametric constant in volts, i is the cell current density, and i_{max} is the limiting current density which is a constant for the cell [Larminie and Dicks 2000]. The H_2 flow rate is calculated using the following relation is

$$W_{H_2} = M_{H_2} \frac{N_{cell} I_{cell}}{2F}, \quad (10)$$

where M_{H_2} is the molar mass of H_2 in Kg/mol, N_{cell} is the number of cells in the stack, I_{cell} is the stack current, and F is the Faraday constant. More details are given in the Appendix.

Li-ion batteries: The DualFoil Fortran program based on a low level electrochemical model [Newman 2004] is used to predict the voltage at the terminal of a battery for a given charge or discharge current. The standalone simulator is modified to work with Simulink through a C-MEX interface.

DC-DC converter: The power input to the DC-DC converter is calculated from the system load current (I_O) and supply voltage that are provided by the embedded system model, and the efficiency characteristics. A polynomial model of the efficiency is derived using measurement data (Fig. 10). The efficiency of the DC-DC converter, η_{DC}, is given by

$$\eta_{DC} = \begin{cases} -3.472E^{-7}{I_O}^3 + 4.316E^{-5}{I_O}^2 + 2.167E^{-3}I_O + 6.16E^{-1}, & I_O < 100mA, \\ -3.384E^{-12}{I_O}^3 + 9.065E^{-9}{I_O}^2 + 4.031E^{-5}I_O + 8.996E^{-1}, & I_O \geq 100mA. \end{cases} \tag{11}$$

Fans: The power consumption of the cathode fan (in Watts) is determined by the required air pressure and is given by

$$P_{cathode-fan} = 0.272p_{cathode} + 0.081, \tag{12}$$

where $p_{cathode}$ is pressure in inches of water (inch H_2O).

The cooling fan power consumption is also dependent on the air pressure, and is given by

$$P_{cooling-fan} = 0.104f_{cooling} - 1.481, \tag{13}$$

where $f_{cooling}$ is air flow rate in CFM[1]. The current simulator does not consider high-pressure air pumps (>4 psig), where the fan is of type diaphragm or piston, and consumes higher power.

Fuel pump: The fuel pump in the simulator is a motor- and gear-driven pump. The power consumption of the fuel pump is dependent on the fuel (10% $NaBH_4$ solution) flow rate, and is given by

$$P_{fuel-pump} = 7.27E^{-3}\nu_{fuel} + 4E^{-2}, \tag{14}$$

where ν_{fuel} is flow rate in ml/min.

Purge valve: The purge valve power consumption is given by

$$P_{purge-valve} = 0.67\frac{\tau_{on}}{\tau_{period}}, \tag{15}$$

where τ_{on} and τ_{period} are the duration of the active state of the purge valve, and the period of the purge operation, respectively.

CMS: This module contains the control policies of all the controller components and has been implemented using the Matlab S-function. The power consumption of the CMS is mostly due to the TI MSP430 microprocessor and the analog-to-digital converters. The power consumption is 84 mW when it is in active mode, and only 8 mW when it is in idle mode.

Fuel processor and H_2 pressure calculator: These modules are strongly dependent on the mechanism of the H_2 generator including the catalyst use, the capacity of the reaction

[1] 1 CFM denotes 28.3 l/min flow rate.

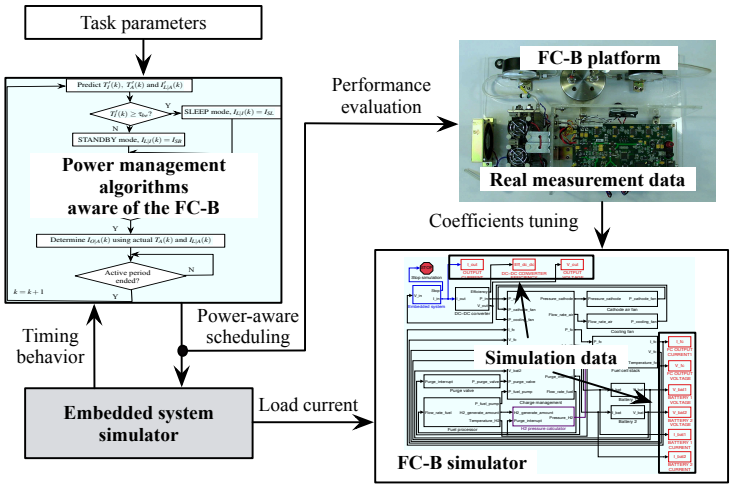

Fig. 13. Power management policy development for embedded systems power by an FC-Bh system.

chamber, temperature of the reaction chamber, and so forth. The current FC-Bh system simulator assumes that the H_2 supply comes from a high-pressure H_2 tank, and that a gas regulator is used to ensure a constant H_2 pressure.

Embedded system: The embedded system model generates the load current profile which is fed into the FC-Bh system simulator. In fact, it can be used in conjunction with any kind of embedded system simulator that is able to provide the power profile of the different tasks.

Power management policy development environment: Fig. 13 illustrates the proposed environment for developing power (energy) management policy for an FC-Bh system. Details of the energy optimization framework is described in Section 6. For faster feedback, we use the simulator during the policy development stage. Once we confirm a policy using the simulator, we actually measure its performance on the FC-Bh system platform.

6. ENERGY OPTIMIZATION FOR AN FC-BH SYSTEM

Extending the operational lifetime of embedded systems used in portable applications is usually achieved by reducing their energy consumption. DPM is a well-known and widely-used energy reduction technique which puts the embedded system into a lower power state to save energy when the idle time is long enough. Research in this area includes prediction of future idle periods [Hwang and Wu 1997; Srivastava et al. 1996; Chung et al. 1999], stochastic control [Benini et al. 2000; Rong and Pedram 2006], aggregation of small idle times to get longer idle durations [Jejurikar et al. 2004; Lu et al. 2000a], etc. However, most of the previous work was geared for battery-powred systems, which can automatically track the changes in the load demand. In such systems, lowering the load energy consumption translates to lowering the energy drawn from the batteries. However, this is not the case when the system is powered by the FC-Bh system. The FC cannot follow the

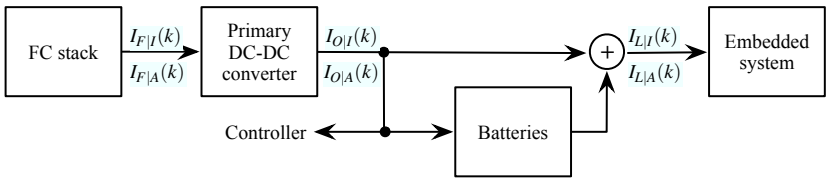

Fig. 14. Current flow in the FC-Bh system for the FC-DPM formulation.

load changes automatically and thus the FC current has to be actively controlled to minimize the fuel consumption. Furthermore, the fuel flow rate control is a lot slower than the load fluctuations, and so the fuel flow rate control is not done during task execution but rather at the inter-task boundaries.

In this section, we present the fuel-aware DPM policy that reduces the energy consumption by explicitly considering the characteristics of the FC-Bh system investigated in Section 4.2. This was presented in [Zhuo et al. 2007a] and has been included here for the sake of completeness. The goal is to maximize the lifetime of the FC-Bh system for a given amount of fuel, i.e., minimization of the fuel consumption. We first present an optimization framework to determine the FC current to achieve this goal when the FC-Bh system can be represented by a linear efficiency function $\eta_s = \alpha - \beta I_O$ (as shown in Figure 11(b)). Next we apply the optimization framework on top of a well-known prediction based DPM technique and develop a fuel-aware DPM policy, *FC-DPM*. The experiments based on real MPEG encoding traces demonstrate that *FC-DPM* can improve the operational lifetime of the fuel cell significantly compared to two baseline DPM policies.

6.1 Definitions

The load profile of the embedded system is represented by a sequence of task slots. We assume, without loss of generality, that each task slot consists of an idle slot followed by an active slot. For a given task slot, k, we denote the length of the idle slot as $T_I(k)$, the load current as $I_{L|I}(k)$, the FC stack current as $I_{F|I}(k)$, and the current after the primary DC-DC converter as $I_{O|I}(k)$. Similarly, $T_A(k)$, $I_{L|A}(k)$, $I_{F|A}(k)$ and $I_{O|A}(k)$ denote the length of the active task and the corresponding load current, FC stack current and current after the primary DC-DC converter, respectively. Note that the FC stack current, I_F (a simplified notation of $I_{F|I}(k)$ or $I_{F|A}(k)$), and the current after the primary DC-DC converter, I_O, are different; I_F is directly proportional to the fuel consumption rate and it is related to I_O by Equation (8). To simplify the analytical formulations in this paper, we modified the current flow model of the FC-Bh system which has an autoregressive (AR) configuration of the primary DC-DC converter and battery (Fig. 4) to a moving-average (MA) configuration (Fig. 14), assuming that there is no loss during battery charging.

Without loss of generality, we assume that the DPM-enabled embedded system has three power modes: RUN, STANDBY and SLEEP. The power mode during the active slot is always set to RUN, and the corresponding load current, $I_{L|A}(k)$, depends on the task specifications. The power mode during the idle slot is either STANDBY or SLEEP and determined by the DPM policy. The load current in the idle slot is $I_{L|I}(k) = I_{SB}$ or $I_{L|I}(k) = I_{SL}$, where I_{SB} and I_{SL} are embedded system currents in the STANDBY mode and SLEEP mode, respectively. Recall that to enter SLEEP mode, the idle slot must be longer than the

Table I. Nomenclature

Symbols	Description
I_{SB}, I_{SL}	Load current in STANDBY and SLEEP modes
I_{PD}, I_{WU}	Load current when entering (power down) or exiting (wake up) SLE EP mode
τ_{PD}, τ_{WU}	Transition delay when entering or exiting SLEEP mode
τ_{be}	Break-even time of the DPM
$T_I(k)$, $T_A(k)$	Length of k-th idle and active slots
$I_{L\|I}(k)$, $I_{L\|A}(k)$	Load current in the k-th idle and the active slots
$I_{O\|I}(k)$, $I_{O\|A}(k)$	Primary DC-DC converter output current in the k-th idl e and active slots
$I_{F\|I}(k)$, $I_{F\|A}(k)$	FC stack current in the k-th idle and active slots
α, β	Coefficients of the system efficiency
C_{max}	Capacity of the charge storage element
$Q_{ini}(k), Q_{end}(k)$	Stored charge at the beginning and the end of the task sl ot

DPM break-even time, i.e., $T_I \geq \tau_{be}$ [Benini et al. 2000].

In practice, we assume that there is no direct transition between SLEEP mode and RUN mode, i.e., the transition must go through a STANDBY mode. The transition overhead between RUN and STANDBY modes can be accounted for by assuming that the load current is $I_{L|A}(k)$ for an extended duration of $T_A(k)$. The transition overhead between SLEEP mode and STANDBY mode is represented as follows. The transition delay to the SLEEP mode is τ_{PD} (PD: power down) and the corresponding load current is I_{PD}; the transition delay from the SLEEP mode is τ_{WU} (WU: wake up) and the corresponding load current is I_{WU}.

The maximum charge storage capacity of the FC-Bh system is C_{max}. The state of the charge storage element at the beginning and end of k-th task slot are denoted by $Q_{ini}(k)$ and $Q_{end}(k)$, respectively. Table I summarizes the definitions mentioned above.

6.2 Determination of the fuel-efficient $I_{F|I}(k)$ and $I_{F|A}(k)$

Here we describe the optimization process to determine the fuel-efficient $I_{F|I}(k)$ and $I_{F|A}(k)$ for a single task slot k. We make the following assumptions based on the real system implementation: i) we change the FC current only when there is a power mode transition in the embedded system, i.e., $I_{F|I}(k)$ and $I_{F|A}(k)$ are constant values for each k, and ii) the load current profile, $I_{L|I}(k)$ and $I_{L|A}(k)$ is determined by the DPM policy and is known a priori.

The goal is to minimize the fuel consumption, $\mathcal{C}$, which is proportional to $I_{F|I}(k)T_I(k) + I_{F|A}(k)T_A(k)$. Recall that the amount of FC current is proportional to the fuel consumption (from Equations (1) and (2)). Utilizing the relationship between the FC current and the DC-DC output current shown in Equation (8), the cost function is given by

$$\text{minimize} : \mathcal{C}\left(I_{O|I}(k), I_{O|A}(k)\right) = \left(\frac{I_{O|I}(k)}{\alpha - \beta I_{O|I}(k)}\right) T_I(k) + \left(\frac{I_{O|A}k}{\alpha - \beta I_{O|A}(k)}\right) T_A(k). \quad (16)$$

We first begin with a simple case where i) the load following range of the FC is unlimited, ii) $C_{max} = \infty$, and iii) $\tau_{PD} = \tau_{WU} = 0$ and $I_{PD} = I_{WU} = 0$. We further assume that we maintain $Q_{end}(k) = Q_{ini}(k)$ in each task slot for system stability. The charge stored into the charge storage unit during the idle slot is given by $\left(I_{O|I}(k) - I_{L|I}(k)\right) \times T_I(k)$, and the charge withdrawn from the charge storage unit during the active slot is $(I_{L|A}(k) - I_{O|A}(k)) \times$

$T_A(k)$. Since we assume that $Q_{ini}(k) = Q_{end}(k)$, we have the additional constraint,

$$(I_{O|I}(k) - I_{L|I}(k)) \times T_I(k) = (I_{L|A}(k) - I_{O|A}(k)) \times T_A(k). \quad (17)$$

The Lagrange multiplier method can be used to solve the constraint optimization problem, and the solution is given by

$$I_{O|I}(k) = I_{O|A}(k) = \frac{I_{L|I}(k)T_I(k) + I_{L|A}(k)T_A(k)}{T_I(k) + T_A(k)}. \quad (18)$$

The FC stack current, I_F, can be calculated by Equation (8), i .e., $I_F = \frac{0.32 \times I_O}{\alpha - \beta I_O}$.

Limited load following range: The FC load following range is limited, and expressed as $I_O \in [0.1\ A, 1.2\ A]$ for the system under consideration. Thus if $I_{O|I}$ and $I_{O|A}$ given by Equation (18) are out of range, we set them to the closest boundary value in the load following range (i.e., 0.1 A or 1.2 A).

Capacity limitation: If C_{max} is finite, we have the following additional constraint:

$$Q_{ini}(k) + (I_{O|I}(k) - I_{L|I}(k)) \times T_I(k) \leq C_{max}. \quad (19)$$

In this case, we first derive $I_{O|I}(k)$ using Equation (18) and check if the inequality in Equation (19) is satisfied. If not, we reduce $I_{O|I}(k)$ such that $(I_{O|I}(k) - I_{L|I}(k)) \times T_I(k) = C_{max}$, and then calculate $I_{O|A}(k)$ using Equation (17). Equation (19) could be violated in the extreme case where the lower bound of the load following range is still too high. In such a case, the excess current is dissipated though the bleeder by-pass.

$\mathbf{Q_{end} \neq Q_{ini}}$: If $Q_{end}(k) = Q_{ini}(k)$ for each task slot, then $Q_{ini}(k) = Q_{ini}(1)$ since $Q_{ini}(k+1) = Q_{end}(k)$. However, due to factors such as limited load following range, limited charge capacity, and differences between the actual load profile and the predicted profile, $Q_{ini}(k)$ may not be equal to $Q_{ini}(1)$. For the current task slot, $Q_{end}(k)$ is an expected value (future) and is set to $Q_{ini}(1)$, while $Q_{ini}(k)$ is a known value. The constraint in Equation (17) is now transformed to

$$Q_{ini}(k) + (I_{O|I}(k) - I_{L|I}(k)) \times T_I(k) = (I_{L|A}(k) - I_{O|A}(k)) \times T_A(k) + Q_{end}(k) \quad (20)$$

We can solve this problem by following the same method used in the case when $Q_{ini}(k) = Q_{end}(k)$.

Transition overhead: In Equations (16) and (17), we ignored the time and energy overhead during the DPM state transition. Recall that the transition overhead between STANDBY and RUN modes has been absorbed by extending the active slot. Here we consider how to take into account the transition overhead between SLEEP mode and STANDBY mode.

For the k-th idle slot, we define a binary variable δ such that $\delta = 1$ when the embedded system is sent to the SLEEP mode, and $\delta = 0$ when it stays in the STANDBY mode. The transition delay from the idle slot to the active slot is $\delta \times \tau_{WU}$, and the transition energy is proportional to $\delta \times I_{WU} \times \tau_{WU}$. We conservatively assume that the next idle slot is in SLEEP mode, and the mode transition delay and energy are represented by τ_{PD} and $I_{PD} \times \tau_{PD}$, respectively. We set the DC-DC output current during the state transition to

$I_{O|A}(k)$. The new cost function is given by

$$\begin{aligned}\text{minimize} : \bar{C}(I_{O|I}(k), I_{O|A}(k)) = & \left(\frac{I_{O|I}(k)}{\alpha - \beta I_{O|I}(k)}\right) T_I(k) \\ & + \left(\frac{I_{O|A}(k)}{\alpha - \beta I_{O|A}(k)}\right) (T_A(k) + \delta\tau_{WU} + \tau_{PD}).\end{aligned} \tag{21}$$

Equation (17) is now modified to

$$\begin{aligned}&(I_{O|I}(k) - I_{L|I}(k)) \times T_I(k) = \\ &\qquad (I_{L|A}(k)T_A(k) + \delta I_{WU}\tau_{WU} + I_{PD}\tau_{PD}) - I_{O|A}(k) \times (T_A(k) + \delta\tau_{WU} + \tau_{PD}).\end{aligned} \tag{22}$$

A method similar to that outlined earlier is used to solve this optimization problem. We can easily take into account the capacity constraint, C_{max}, as well as non-zero Q_{ini} and Q_{end} as described earlier.

6.3 Fuel-efficient DPM

Section 6.2 described how to set I_F, i.e., the fuel flow rate, such that the fuel consumption is minimized when the load profile is given. However, the load profile changes dynamically and cannot be known a priori in realtime systems. In this section, we show how to modify the conventional prediction-based DPM policy for an embedded system powered by the FC-Bh system. The proposed algorithm *FC-DPM* jointly controls the power state of the embedded system and the fuel flow rate of the FC-Bh system such that the fuel consumption is minimized.

DPM on embedded systems: Our algorithm can be built on top of any conventional DPM policy that aims at energy reduction of the embedded system. This is because a policy that reduces energy consumption of the embedded system does not conflict with the fuel-efficient I_F setting, as shown below.

The energy consumption of the embedded system for a task slot k is $V_O \times (I_{L|I}(k) \times T_I(k) + I_{L|A}(k) \times T_A(k))$ when we ignore the transition overhead. Since V_O is constant, if we use the policy in Section 6.2 to determine the fuel cell output current, a lower energy consumption of the embedded system transforms to a smaller I_O according to Equation (18), a smaller I_F according to Equation (8), and eventually a lower fuel consumption.

We chose a simple DPM policy proposed in [Hwang and Wu 1997] for the baseline policy. The predicted idle slot period, $T_I'(k)$, is a linear combination of the predicted duration and the actual duration of the previous idle period,

$$T_I'(k) = \rho \times T_I'(k-1) + (1-\rho) \times T_I(k-1). \tag{23}$$

If $T_I'(k) > \tau_{be}$, the embedded system is put into SLEEP mode.

$\mathbf{I_F}$ control: The value of the fuel-efficient I_F is based on the predicted duration of the next active slot, $T_A'(k)$, as well as $T_I'(k)$. This is the one of key differences between the proposed fuel-efficient DPM and the conventional DPMs that rely solely on $T_I'(k)$.

We propose a policy similar to [Hwang and Wu 1997] to get the predicted value of $T_A'(k)$ by the following equation:

$$T_A'(k) = \gamma T_A'(k-1) + (1-\gamma) T_A(k-1). \tag{24}$$

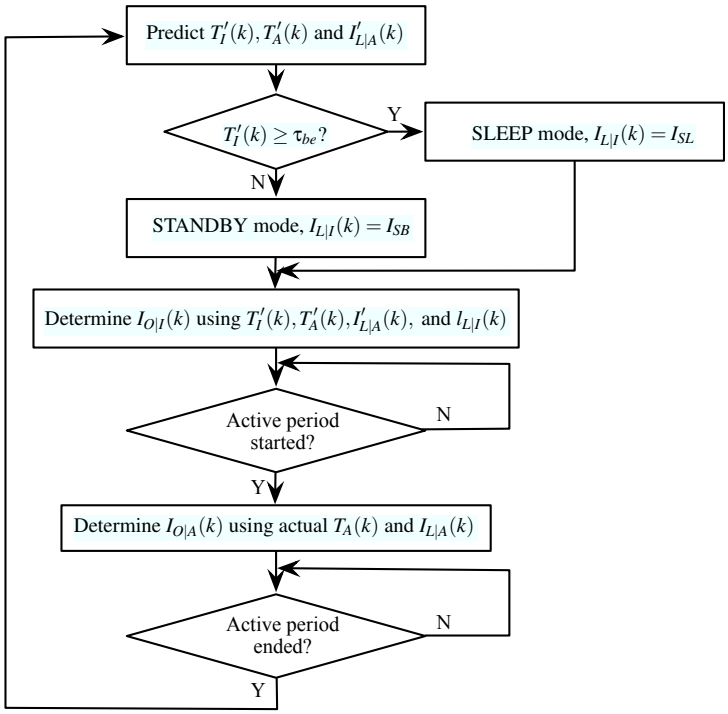

Fig. 15. Outline of Algorithm *FC-DPM*.

The values of ρ and γ could be different, depending on the pre-known pattern of the load profile. Once we have $T_I'(k)$ and $T_A'(k)$, we determine $I_{F|I}(k)$ using the method described in Section 6.2. After the system resumes RUN mode, we calculate $I_{F|A}(k)$ according to the actual values of $T_A(k)$ and $I_{L|A}(k)$.

In this paper, we only mention how to predict $T_A'(k)$, which is under the assumption that the $I_{L|A}(k)$ is not different from $I_{L|A}(k-1)$. In reality, $I_{L|A}(k)$ changes with k, and so we should use a predicted value $I_{L|A}'(k)$, which could be estimated based on the load current of the past active slots and/or task characteristics. The outline of Algorithm *FC-DPM* is shown in Figure 15.

6.4 Experimental results

Experimental setup: The experimental setup is based on the FC-Bh system platform with a BCS 20 W FC stack and a charge storage with $C_{max} = 100$ mA-min and 12 V, which i s equivalent to a 1 F super capacitor.

Applications: The target application is MPEG encoding and writing to a DVD ROM in a DVD camcorder. The DVD camcorder is composed of a 4X speed DVD writer, an MPEG encoder, a 16 MB buffer, and an LCD (which is assumed to be turned off at all times). The power states and state transitions for the camcorder are shown in Figure 16, and described below:

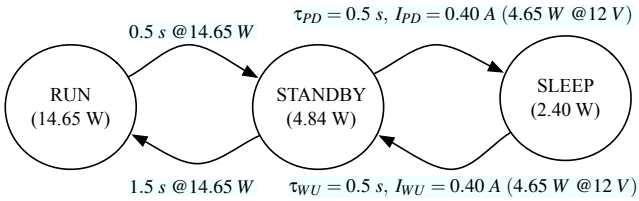

Fig. 16. The power state abstraction of the DVD camcorder.

(1) RUN mode: The buffer is full and the DVD writer performs the writing operation. The load power consumption is 14.65 W, and the active period is 3.03 s (corresponding to 16 MB buffer size, and 5.28 MB/s writing speed). The transition from STANDBY mode to RUN mode takes 1.5 s, and from RUN mode to STANDBY mode takes 0.5 s. The load power consumption during the state transitions is assumed to be the same as the power in the active period.

(2) STANDBY mode: The DVD finishes writing, and the encoder starts working. The load power consumption is 4.84 W. The length of the idle period is varied from 8 s to 20 s, depending on the characteristics of the MPEG frames.

(3) SLEEP mode: The encoder keeps working but the DVD is in SLEEP mode. The load power is 2.4 W. The state transition from SLEEP mode to STANDBY mode, and vice versa, takes 0.5 s and consumes 4.84 W power. The break-even time is $\tau_{be} = \tau_{PD} + \tau_{WU} = 1$ s.

We compare the performance of Algorithm *FC-DPM* with the following algorithms.

(1) Conv-DPM: This is conventional DPM policy for the hybrid system where the FC has no fuel flow control. This means that the FC current is always set to a constant value. Here $I_F = 1.3$ A, corresponding to the upper bound of the load following range ($I_O = 1.2$ A).

(2) ASAP-DPM: This is a DPM policy that utilizes the load following capability of the FC and matches $I_{O|I}(k)$ to $I_{L|I}(k)$, and $I_{O|A}(k)$ to $I_{L|A}(k)$ as closely as possible. If the amount of charge in the charge storage unit drops below $\frac{1}{2}C_{max}$, it is recharged to C_{max} as soon as possible by letting the FC deliver the highest current in the successive task slots.

We apply the DPM policies for a 28 min trace of the DVD camcorder. The prediction factor for the idle period is set to $\rho = 0.5$. The prediction for the active period is not necessary here since the active period length is fixed. We first run the simulation with the efficiency coefficients of $\alpha = 0.46$ and $\beta = 0.13$, which corresponds to the curve with 2 W static power in Figure 11(b). Figure 17 shows 0 to 300 s simulation of the following current profiles: (a) the load profile of the DVD camcorder, (b) I_O under *ASAP-DPM*, and (c) I_O under *FC-DPM*. We did not include the profile of *Conv-DPM* since I_O is always 1.2 A. As we can see from the current profiles, the load current under *ASAP-DPM* follows the load current of the DVD camcorder very well. However, the large variation between $I_{L|I}(k)$ and $I_{L|A}(k)$ results in larger fuel consumption. The load current under *FC-DPM* is much more flatter and results in the lowest fuel consumption due to the convexity of Equation (8).

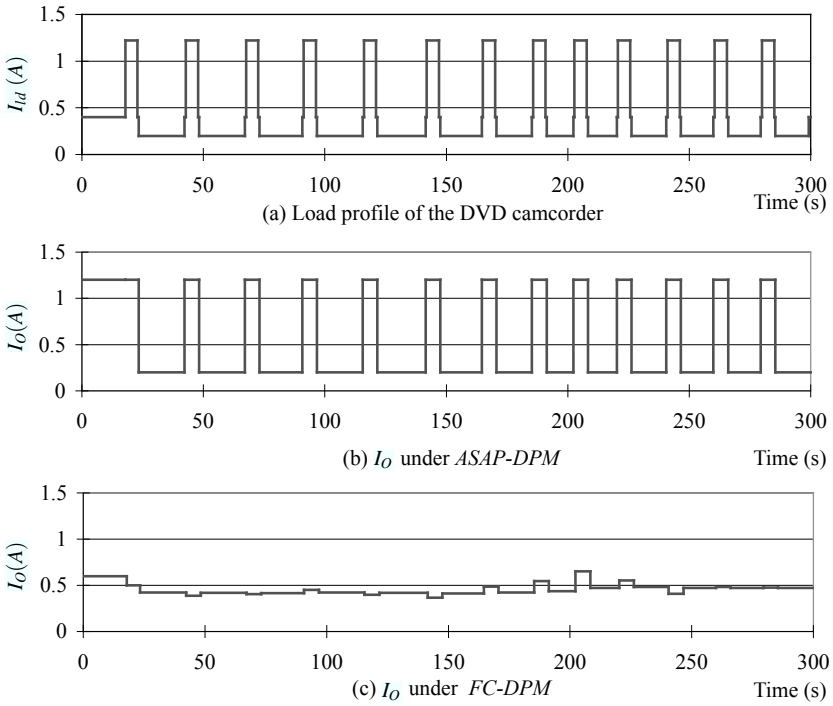

Fig. 17. The current profiles of the DVD experiment

Table II. Normalized fuel consumption for the DVD example

DPM policy	Conv-DPM	ASAP-DPM	FC-DPM
$\alpha = 0.46, \beta = 0.13$	100%	40.9%	31.1%
$\alpha = 0.48, \beta = 0.1$	100%	41.9%	34.2%

The fuel consumption corresponding to the different DPM policies is shown in the first row of Table II. The values have been normalized to that of *Conv-DPM*. The fuel consumption of *ASAP-DPM* and *FC-DPM* is significantly lower than that of *Conv-DPM* because both the policies exploit the load following capability of the power source. *FC-DPM* reduces the fuel consumption furthermore since it determines I_O based on the FC system efficiency characteristics. The normalized fuel consumption of *FC-DPM* is as low as 31.1% compared to that of *Conv-DPM*. If we compare *FC-DPM* and *ASAP-DPM*, *FC-DPM* saves 24% more fuel. Since the operational lifetime with a given about of fuel, is inversely proportional to the fuel consumption, *FC-DPM* has a lifetime that is 31.5% longer than that of *ASAP-DPM*.

Next, we keep all the conditions the same but use another FC configuration where $\alpha = 0.48$ and $\beta = 0.1$. This corresponds to the curve with 0.8 W static power in Figure 11(b). The normalized fuel consumption of the three policies is shown in the second row of Table II. The result shows that the performance of *FC-DPM* is consistently superior. The fuel savings is slightly smaller because the slope of the efficiency curve is flatter than that of

the previous case. The lifetime achieved by *FC-DPM* is now 22.5% longer than that of *ASAP-DPM*.

7. CONCLUSIONS AND FUTURE WORK

FCs are one of the most promising next generation energy sources for human-portable applications. They have very high energy density, and are also safe and environmentally clean. However, due to their limited power capacity, they are inefficient as a stand-alone power source. An FC-Bh (FC-battery hybrid) system is very efficient since it has the energy density of the FC and power density of the battery. Such a system introduces nonlinearities and requires development of novel charge management policies and new power management policies.

In this paper, we have described the design and implementation of a prototype FC-Bh system for use in portable applications. The working platform includes a 20 W, 20 stack PEMFC stack with a cathode air fan, a cooling fan and a purge valve for water management, a sodium borohydride-based H_2 generator, and a CMS with dual Li-ion batteries and novel discharge selection circuits (DTC). We have also designed a Matlab/Simulink simulator which serves as an alternate experimental platform. The analytical models used for each of the components in the simulator have been tuned with the measurement data. We have analyzed the FC-Bh system efficiency as a function of the FC stack efficiency, DC-DC converter efficiency, the power consumption of the controller components such as fans, etc.

Next, we addressed the problem of dynamic power management (DPM) for embedded systems powered by an FC-Bh system. The objective here is to minimize the fuel consumption, and thereby extend the operational lifetime. Due to the unique power and efficiency characteristics of the hybrid system, conventional DPM cannot be directly used. To address this problem, we developed a charge-based optimization framework to determine the FC output current such that the fuel consumption is minimized. Next we utilized this framework on top of a prediction based DPM scheme to develop a fuel-efficient DPM algorithm, *FC-DPM*, for run time operation. The performance of the proposed algorithm was evaluated on both real MEPG decoding/writing traces of a DVD camcorder. Experimental results showed up to 32% extension of the operational lifetime compared to a competing algorithm.

8. ACKNOWLEDGMENT

This work was supported in part by the Institute of Computer Technology (ICT) at SNU, the Brain Korea 21 Project, LG Yonam Foundation in Korea, the NSF Center for Low Power Electronics under Grant EC-9523338, NSF CSR-EHS 0509540 and the Consortium for Embedded Systems, ASU.

We give special thanks to Dr. Ken Han and his colleagues at Korean Institute of Industrial Technology (KITECH), and Dr. Dominic Gervasio and his colleagues at Arizona State University (ASU), for their support in providing us with the PEMFC stack and the H_2 generator.

9. APPENDIX

9.1 Static characteristics

In this section we present a few details of how the FC voltage is related to the current. Using thermodynamic values of the standard-state entropy change, the internal voltage or Nerst potential of one FC, E_{fc} is given by [Amphlett et al. 1995]:

$$\begin{aligned} E_{fc} &= 1.229 - 0.85 \times 10^{-3}(T_{fc} - 298.15) \\ &\quad +4.3085 \times 10^{-5} T_{fc} \left(\ln(P_{H_2}) + \frac{1}{2} \ln(P_{O_2}) \right), \end{aligned} \tag{25}$$

where T_{fc} is the temperature of the FC in Kelvin (K), and P_{H_2} and P_{O_2} are the partial pressure of the H_2 and O_2, expressed in atm. This is the theoretical maximum voltage can be harnessed from a cell. The characteristic shape of the voltage and current density curve for a FC can be explained using three types of losses, namely, activation loss, ohmic loss and concentration loss. Each of these are summarized here.

The activation loss is caused by the slowness of the reactions taking place on the surface of the electrodes. The activation loss or activation overvoltage arises from the need to move electrons, and to break and form the chemical bonds in the anode and the cathode [Lee et al. 1998]. Part of the available energy is lost in driving the chemical reaction that transfers the electrons to and from the electrodes [Larminie and Dicks 2000]. For the low temperature PEM FCs, the activation overvoltage v_a can be described using the Tafel equation,

$$v_a = \frac{RT}{2\alpha F} \cdot ln(\frac{i}{i_0}), \tag{26}$$

where R is the gas constant, T is the stack temperature, α is the charge transfer coefficient which is different for the anode and the cathode, and i_0 is the exchange current density which is again different for the anode and the cathode [Larminie and Dicks 2000]. The simulation environment uses this model for the activation losses using published values for α and i_0. Authors in [Pukrushpan et al. 2004] have used a model of the form as below

$$v_a = V_0 + V_1(1 - e^{-c_1 i}), \tag{27}$$

where V_0 is the open-circuit voltage drop, and V_1 and c_1 are constants, which can be determined by nonlinear regression with empirical methods. The activation overvoltage depends strongly on the temperature [Kordesch and Simader 1996] and the O_2 partial pressure [Amphlett et al. 1995].

The ohmic loss has two components: resistance to the flow of electrons through the material of the electrode and resistance to the flow of protons (H^+) through the membrane. The membrane resistance is a function of the water content in the membrane and the stack current. The voltage drop that corresponds to the ohmic loss is proportional to the current.

$$v_\Omega = iR_\Omega, \tag{28}$$

$$R_\Omega = (R_{electron} + R_{proton}), \tag{29}$$

$$R_{proton} = \frac{r_M \cdot l}{A}, \tag{30}$$

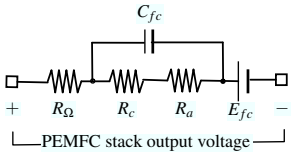

Fig. 18. Equivalent circuit of the PEMFC stack.

$$r_M = \frac{181.6\left(1+0.03\left(\frac{i}{A}\right)+0.062\left(\frac{T}{303}\right)^2\left(\frac{i}{A}\right)^{2.5}\right)}{\left(\lambda-0.634-3\left(\frac{i}{A}\right)\right)\exp\left(4.18\left(\frac{T-303}{T}\right)\right)}, \tag{31}$$

where λ is a measure of the water content in the membrane [Amphlett et al. 1995]. A value of 14 indicates a well hydrated membrane, l is the thickness of the membrane, A is the membrane area of the cell, and i is the stack current. The simulation environment takes λ and $R_{electron}$ as a configurable parameter and computes the ohmic loss in the cell.

The concentration loss results from the change in concentration of the reactants at the surface of the electrodes as the fuel is consumed. At high current density operation, this loss is significant and is often called mass transport loss. The voltage drop amount due to the concentration losses is given by [Guzzella 1999]

$$v_c = i\left(c_2\frac{i}{i_{\max}}\right)^{c_3}, \tag{32}$$

where c_2, c_3, and $i_{\max}$ are constants that depend on the temperature and the reactant partial pressure. Authors in [Larminie and Dicks 2000] also suggest another model for the concentration loss

$$v_c = B\cdot\ln\left(1-\frac{i}{i_{max}}\right), \tag{33}$$

where B is a parametric constant in volts, i is the cell current density, and i_{max} is the limiting current density which is a constant for the cell. The simulation environment uses this model to approximate the concentration losses.

Finally, the following equation describes the static operating voltage of a FC at a current density i.

$$\begin{aligned} v_{fc} &= E_{fc} - v_a - v_\Omega - v_c \\ &= E_{fc} - \left(V_0 + V_1(1-e^{-c_1 i})\right) - iR_\Omega - i\left(c_2\frac{i}{i_{\max}}\right)^{c_3}, \end{aligned} \tag{34}$$

The static stack operating voltage can be calculated by multiplying the cell voltage v_{fc} by the number of stacked cells.

9.2 Dynamic characteristics

The charge double layer is an important concept that helps in understanding the dynamic electrical behavior of the FC [Larminie and Dicks 2000]. Whenever two different materials are in contact, there is a charge layer build-up at the interface or a charge transfer occurs

from one layer to the other. In the electrochemical systems, the charge double layer forms in part due to diffusion effects and in part due to the reaction between the electrons in the electrodes and the ions in the electrolyte. The layer of charge on or near the electrode-electrolyte interface acts as a storage of electrical charge, and behaves like an electrical capacitor. Its capacitance is given by

$$C = \varepsilon \frac{A}{d}, \tag{35}$$

where ε is the electrical permittivity, A is the real surface area of the electrode which is several thousand times greater than its length $\times$ width, and d is the separation of the plates which is very small, typically only a few nanometers [Larminie and Dicks 2000]. The result is that the capacitance is of the order of a few Farads. Therefore, when the current suddenly changes, it takes some time before the activation overvoltage and the concentration overvoltage follow the change in the current. On the other hand, the ohmic voltage drop responds instantaneously to a change in the current. Thus, the equivalent circuit in Fig. 18 can be used to model the dynamic behavior of the FC. From Equation (27) and (32), we can define the activation resistance R_a and the concentration resistance R_c.

$$\begin{aligned} R_a &= \frac{1}{i}\left(V_0 + V_1(1 - e^{-c_1 i})\right), \\ R_c &= \left(c_2 \frac{i}{i_{\max}}\right)^{c_3}, \end{aligned} \tag{36}$$

Therefore, the dynamic FC voltage behavior can be described by

$$\begin{aligned} C_{fc}\frac{dv_c}{dt} + \frac{v_c - V_0}{R_a + R_c} &= i, \\ v_{fc} &= E_{fc} - v_c - iR_\Omega, \end{aligned} \tag{37}$$

where v_c is the voltage of the capacitor.

Fig. 18 shows the equivalent circuit of the FC that can be used to explain its dynamic characteristics. In the circuit diagram, R_a and R_c are equivalent resistance of v_a and v_c, respectively. We have characterized the PEMFC stack used in our platform using these parameters.

REFERENCES

2006. The BCS fuel cell stack #10-20 document. *http://bcsfuelcells.com*.

2007. The JSW metal hydride storage. *http://www.fcexpo.jp/english*.

2007. The STAR prototype diaphragm micro pump SDMP306. *http://www.star-m.jp/eng*.

AKBARI, M. H. 2005. Pem fuel cell systems for electric power generatiuon: An overview. In *Proceedings International Hydrogen Energy Congress and Exhibition IHEC 2005*.

AMPHLETT, J. C., BAUMERT, R. M., MANN, R. F., PEPPLEY, B. A., AND ROBERGE, P. R. 1995. Performance modeling of the Ballard Mark IV solid polymer electrolyte fuel cell. *Journal of Electrochemical Society 142,* 1 (Jan.), 9–15.

BENINI, L., BOGLIOLO, A., AND DE MICHELI, G. 2000. A survey of design techniques for system-level dynamic power management. *IEEE Transactions on VLSI Systems 8*, 299–316.

BENINI, L. AND DE MICHELI, G. 1998. *Dynamic Power Management: Design Techniques and CAD Tools*. Kluwer, Massachussets.

BURD, T. D., PERING, T. A., STRATAKOS, A. J., AND BRODERSEN, R. W. 2000. A dynamic voltage scaled microprocessor system. *IEEE Journal of Solid-State Circuits 35,* 11 (Nov.), 1571–1580.

CHANDRASENA, L. H. AND LIEBELT, M. J. 2000. Energy minimization in dynamic supply voltage scaling systems using data dependent voltage level selection. In *Proceedings of the International Symposium on Circuits and Systems*. 525–528.

CHO, Y., CHANG, N., CHAKRABARTI, C., AND VRUDHULA, S. 2006. High-level power management of embedded systems with application-specific energy cost functions. In *Proceedings of the IEEE Design Automation Conference*. 568–573.

CHOI, K., SOMA, R., AND PEDRAM, M. 2004. Off-chip latency-driven dynamic voltage and frequency scaling for an MPEG decoding. In *Proceedings of the IEEE Design Automation Conference*. 544–549.

CHUNG, E. Y., BENINI, L., AND DE MICHELI, G. 1999. Dynamic power management using adaptive learning tree. In *Proceedings of the IEEE International Conference on Computer Aided Design (ICCAD)*. 274–279.

GAO, L., JIANG, Z., AND DOUGAL, R. A. 2005. Evaluation of active hybrid fuel cell/battery power sources. *IEEE Transactions on Aeorspace and Electronic Systems 41,* 1 (Jan.), 346–355.

GAO, W. 2005. Performance comparison of a fuel cell-battery hybrid powertrain and a fuel cell-ultracapacitor hybrid powertrain. *IEEE Transactions on Vehicular Technology 54,* 3 (May), 846–855.

GERVASIO, D., TASIC, S., AND ZENHAUSERN, F. 2005. A room temperature micro-hydrogen generator. *Journal of Power Sources 149*, 15–21.

GIELNIAK, M. J. AND SHEN, Z. J. 2004. Power management strategy based on game theory for fuel cell hybrid electric vehicles. In *Proceedings of the Vehicular Technology Conference (VTC)*. Vol. 6. 4422–4426.

GUEZENNEC, Y., CHOI, T. Y., PAGANELLI, G., AND RIZZONI, G. 2003. Supervisory control of fuel cell vehicles and its link to overall system efficiency and low-level control requirements. In *Proceedings of the American Control Conference (ACC)*. Vol. 3. 2055–2061.

GUZZELLA, L. 1999. Control oriented modeling of fuel-cell based vehicles. *Presentation in NSF workshop on the integration of modeling and control for automotive systems*.

HWANG, C. H. AND WU, A. 1997. A predictive system shutdown method for energy saving of event-driven computation. In *Proceedings of the IEEE International Conference on Computer Aided Design (ICCAD)*. 28–32.

ISHIHARA, T. AND YASUURA, H. 1998. Voltage scheduling problem for dynamically variable voltage processors. In *Proceedings of the IEEE International Symposium on Low Power Electronics and Design*. 197–202.

JARVIS, L. P., CYGAN, P. J., AND ROBERTS, M. P. 2002. Fuel cell/lithium-ion battery hybrid for manportable applications. In *Proceedings of the Battery Conference on Applications and Advances*. 69–72.

JEJURIKAR, R., PEREIRA, C., AND GUPTA, R. 2004. Leakage aware dynamic voltage scaling for real-time embedded systems. In *Proceedings of the IEEE Design Automation Conference*. 275–280.

JIANG, Z., GAO, L., AND DOUGAL, R. A. 2005. Flexible multiobjective control of power converter in active hybrid fule cell/battery power sources. *IEEE Transactions on Power Electronics 20,* 1 (Jan.), 244–253.

KELLY, L. 2004. *Low Power Electronics Design*. CRC Press, Florida.

KIPPLEY, R. H. 2004. Dual input dc-to-dc power converter. *United States Patent Application Publication*, US2004/0004402A1.

KOJIMA, Y. 2005. Hydrogen storage and generation using sodium borohydride. *R&D Review of Toyota CRDL 40*, 31–36.

KORDESCH, K. AND SIMADER, G. 1996. *Fuel cells and their applications*. VCH, Weinheim ,Germany.

LARMINIE, J. AND DICKS, A. 2000. *Fuel cell systems explained*. John Wiley & Sons, LTD.

LEE, J. H., LALK, T. R., AND APPLEBY, A. J. 1998. Modeling electrochemical performance in large scale proton exchange membrane fuel cell stacks. *Journal of Power Sources 70,* 2, 258 –268.

LU, Y., BENINI, L., AND DE MICHELI, G. 2000a. Low-power task scheduling for multiple devices. In *Proceedings of the International Symposium on Hardware/Software Codesign*. 39–43.

LU, Y. H., BENINI, L., AND DE MICHELI, G. 2000b. Requester-aware power reduction. In *International Symposium on System Synthesis*. Stanford University, 18–23.

LU, Y. H., BENINI, L., AND DE MICHELI, G. 2002. Dynamic frequency scaling with buffer insertion for mixed workloads. *IEEE Transactions on Computer-Aided Design 21,* 11 (Nov.), 1284–1305.

MACII, E. 2004. *Ultra Low Power Electronics and Design*. Kluwer, Massachusetts.

MAYNARD, H. L. AND MEYERS, J. P. 2002. Miniature fuel cells for portable power: Design considerations and challenges. *Journal of Vacuum Science & Technology 20,* 4 (July), 1287–1297.

MCGRATH, K. 2006. Improved low temperature electrical performance employing a pt/nano-cobalt cathode electrode. *QuantumSphere Inc.*.

NASIRI, A., RIMMALAPUDI, V. S., EMADI, A., CHMIELEWSKI, D. J., AND AL-HALLAJ, S. 2004a. Active control of a hybrid fuel cell-battery system. In *Proceedings of the International Power Electronics and Motion Control Conference (IPEMC)*. 491–496.

NASIRI, A., RIMMALAPUDI, V. S., EMADI, A., CHMIELEWSKI, D. J., AND AL-HALLAJ, S. 2004b. Active control of a hybrid fuel cell-battery system. In *Proceedings of the International Power Electronics and Motion Control Conference (IPEMC)*. Vol. 2. 491–496.

NEWMAN, J. S. 2004. Fortran programs for simulation of electrochemical systems, dualfoil.f program for lithium battery simulation. *http://www.cchem.berkeley.edu/ jsngrp/fortran.html*.

OZATAY, E., ZILE, B., ANSTROM, J., AND BRENNAN, S. 2004. Power distribution control coordinating ultracapacitors and batteries for electric vehicles. In Proceedings of the American Control Conference (ACC). *Proceedings of the American Control Conference (ACC) 5*, 4716–4721.

PALO, D. R., HOLLADAY, J. D., ROZMIAREK, R. T., GUZMAN-LEONG, C. E., WANG, Y., JIANLI, H., CHIN, Y., DAGLE, R. A., AND BAKER, E. G. 2002. Development of a soldier-portable fuel cell power system. *Journal of Power Sources 108*, 28–34.

PEDRAM, M. AND RABAEY, J. M., Eds. 2002. *Power Aware Design Methodologies*. Kluwer, Massachusetts.

PERROT, P. 1998. *A to Z of Thermodynamics*. Oxford University Press, New York.

PUKRUSHPAN, J. T., STEFANOPOULOU, A. G., AND PENG, H. 2004. *Control of Feul Cell Power Systems: Principles, Modeling Analysis, and Feedback Design*. Springer.

RABAEY, J. M. AND PEDRAM, M., Eds. 1995. *Low Power Design Methodologies*. Kluwer, Massachussets.

RONG, P. AND PEDRAM, M. 2006. Battery-aware power management based on Markovian decision processe. *IEEE Transactions on Computer Aided Design of Integrated Circuits and Systems 25*, 1337–1349.

SIMJEE, F. AND CHOU, P. H. 2006. Everlast: Long-life, supercapacitor operated wireless sensor node. In *Proceedings of the IEEE International Symposium on Low Power Electronics and Design (ISLPED)*. 197–202.

SIMUNIC, T., BENINI, L., ACQUAVIVA, A., GLYNN, P., AND DE MICHELI, G. 2001. Dynamic voltage scaling for portable systems. In *Proceedings of the IEEE Design Automation Conference*. 524–529.

SRIVASTAVA, M., CHANDRAKASAN, A., AND BRODERSEN, R. 1996. Predictive system shutdown and other architectural techniques for energy efficient programmable computation. *IEEE Transactions on VLSI Systems 4*, 42–55.

VAHIDI, A., KOLMANOVSKY, I., AND STEFANOPOULOU, A. 2005. Constraint management in fuel cells: a fast reference governor approach. In Proceedings of the American Control Conference (ACC). *Proceedings of the American Control Conference (ACC) 6*, 3865–3870.

VAHIDI, A., STEFANOPOULOU, A., AND PENG, H. 2004. Model predictive control for starvation prevention in a hybrid fuel cell system. In Proceedings of the American Control Conference (ACC). *Proceedings of the American Control Conference (ACC) 1*, 834–839.

XIE, C., PAVIO, J., HALLMARK, J., BOSTAPH, J., AND FISHER, A. 2002. Key requirements of micro fuel cell system for portable electronics. In *37th Intersociety Energy Conversion Engineering Conference (IECEC)*.

YAN, L., LUO, L., AND JHA, N. K. 2003. Combined dynamic voltage scaling and adaptive body biasing for heterogeneous distributed real-time embedded systems. In *Proceedings of the International Conference on Computer Aided Design*. 30–37.

ZHENG, J. P., JOW, T. R., AND DING, M. S. 2001. Hybrid power sources for pulsed current applications. *IEEE Transactions on Aerospace and Electronic Sys. 37,* 1, 288–292.

ZHUO, J., CHAKRABARTI, C., AND CHANG, N. 2007b. Energy management of dvs-dpm enabled embedded systems powered by fuel cell-battery hybrid source. In *Proceedings of the International Symposium on Low Power Electronics and Design (ISLPED)*.

ZHUO, J., CHAKRABARTI, C., CHANG, N., AND VRUDHULA, S. 2006a. Extending the lifetime of fuel cell based hybrid systems. In *Proceedings of the IEEE Design Automation Conference (DAC)*. 562–567.

ZHUO, J., CHAKRABARTI, C., CHANG, N., AND VRUDHULA, S. 2006b. Maximizing the lifetime of embedded systems powered by fuel cell-battery hybrids. In *Proceedings of the International Symposium on Low Power Electronics and Design (ISLPED)*. 424–429.

ZHUO, J., CHAKRABARTI, C., LEE, K., AND CHANG, N. 2007a. Dynamic power management with hybrid power source. In *Proceedings of the IEEE Design Automation Conference (DAC)*. 871–876.